

Optimizations of the internal structure of the reel of a double rope winder

Jia Fu*

College of Mechanical Engineering, University of Jinan, Jinan, China

Abstract. Due to the shortage of resources, the deep development of resources is imminent, and the superdeep mine hoist plays a leading role in the development process. According to the structure, the hoists can be divided into winding hoists and friction hoists. Winding hoists can be single-rope winding and multi-rope winding. With the increase of mining depth, friction hoists will have the disadvantage of increasing the mass of the tail rope, while wire rope diameter of single-rope winding hoists will increase with the increase of mining depth. So double-rope winding hoists can be used to balance the above two problems. Therefore, this study will use finite element analysis, and treat hoist reel as a uniformly pressurized shell, through the static and modal analysis of reel. Under the maximum static tension, this study gets the reel the force and deformation distribution. Through the change of the internal structure of the reel, it improves the reel force weakness and reduce the reel deformation. By reducing the deformation of the reel, this study tells how to reduce the tension difference of the wire rope. This study will improve the synchronization and stability of the hoisting system and provide an alternative and effective way for the deep development of the resources with the double-rope winding hoists.

Keywords: Reel construction, Finite element analysis, Optimal design, Poor tensioning, Synchronicity

1. Introduction

In recent years, with the rapid growth of demand for mineral resources in social and economic development, the problem of energy shortage has become more and more prominent. Therefore, it has become an important strategic choice for China to search for mineral resources deep inside the earth[1].

The hoists can be divided into two categories according to the different working methods: winding hoists and friction hoists. For friction hoists, as the mining depth increases, the load on the wire rope will be affected by the increased mass of the balanced tail rope. And when the depth exceeds 1200m, in order to ensure the safety of mining, people generally use winding hoists.

The winding hoists are divided into single-rope winding and multi-rope winding, and with the mining depth increase, the single-rope hoists require a higher power to drive motor and a larger diameter reel, which will bring more difficulties in manufacturing and installation, while the multi-rope winding hoists can avoid the relevant shortcomings. As for single-rope hoists, the tail rope is too heavy and the reel diameter is too large, while the steel rope is too thick and not easy to bend. Therefore, this study focuses on the study of multi-rope winding hoists for mining and hoisting in deep wells above 1200m.

Unlike conventional hoisting devices, multi-rope winding hoists have two or more rope zones on the main shaft.

Studies on multi-rope winding hoists include: Wang Ji [2] used Hamilton principle to simulate and analyze the dynamic behavior of multi-rope hoists under unbalanced factors such as transport eccentricity and inconsistent reel radius, and proposed the design principle to restrict the inconformity of dynamic tension between cables. Wu[3] analyzed the dynamic characteristics of super deep multi point winding hoisting system under non-synchronous movements of the wire rope with the help of Lagrange equation. Due to the dynamic load of high speed and heavy load, the wire rope is deformed, thus making the tension difference among the synchronous ropes increase, which can be called *Deformation detuning of the wire rope*, and the *Deformation detuning of the wire rope* makes the synchronous transportation of the hoists more difficult. Under complex working conditions, the wire ropes may break due to uneven force, resulting in the risk of cage fall. In view of the fact that in multi-rope hoists, the problem of differential tension becomes more critical as the number of wound ropes increases[4], the design of a double-rope hoists can balance the problems of oversized single-rope reel diameters and poor multi-rope wire rope tension, so this study focuses on the double-rope hoists.

Studies about wire rope winding tension differences are:

Li[5] studied the difference in tension between the two ropes of a double-rope winding reel due to manufacturing

* Corresponding author: 202030412035@stu.ujn.edu.cn

deviations and differences in the depth of the winding groove, resulting in an unsynchronized lifting of the two ropes. Kaczmarczyk, S [6]-[7] established a vibration differential equation by means of Hamilton's principle to investigate the vibration phenomena of wire ropes in deep wells. Wang Ji[2] analyzed the effect of wire rope length error on the wire rope tension difference by establishing the system dynamics equations. Peng[8] investigated whether COF between wire ropes changes with load and sliding speed under lubricated and dry friction conditions. Yao[9] studied the step changes of hoisting velocity and acceleration caused by coil and layer crossover of rope winding on the LeBus reel.

The existing research on the tension difference of the double-rope winding hoists mainly revolve around the wire rope. The reel will produce a large amount of deformation after the force, so that the wire rope produces a large tension difference, thus affecting the synchronization of the wire rope hoist, but the results of this research are rare. The main findings of the current research on hoist reels are : JM Singly[10]-[11] derived a mathematical theory based on plates and shells and also derived stress distribution functions for welded coils with lengths greater than $\sqrt{4R\delta}$ and for welded coils with lengths less than $\sqrt{4R\delta}$. S.Otto[12] used FEA-Simulations to analyze the radial pressure of a multi-layer wire rope on the reel and the axial thrust on the rope stopper during heavy loads in a hoisting system. P.Dietz [13]-[14] studied the pressure acting on the reel during the winding process of multi-layer wire rope, considering the reduction of inter-layer tension and radial deformation of the wire rope caused by the winding of each layer, and deduced the general formula for calculating the pressure on the reel. Mangalekar S[15] carried out a FEA-Simulations under maximum load conditions on the reel and designed different reel models to derive the optimum reel structure. Wolny [16] studied the stress distribution in webs, barrel shells and other components in a reel and analyzed the hazardous areas on the barrel shell. Jin Minjie [17] analyzed the deformation of the rolls based on the theory of elastic foundation beams. The above research results have been analyzed mainly for single-rope winding hoists, and less analysis has been carried out on the forces on the reels of double-rope winding hoists. Most of the above literatures for the roll deformation amount are obtained by the traditional theory calculation, and the calculation results are rough and have some error. With the continuous development of science and technology, more advanced theories and methods have been obtained. Benjamin Torres[18] proposed the use of a new FBG strain transducer fixed to the surface of the structure under test and showed that the measured strain differed from the actual strain by less than 2.5%. Chen[19] used Pro/E and ANSYS to build a solid model of the reel and solve for the deformation and stress distribution of the reel. Hu[20] integrated use of OptiStruct, HyperMesh software functional modules and used finite element static analysis to identify the shortcomings of the manhole on the reel and adjusted the structure through topology optimization design. Yu [21] analyzed the stress-strain of the reel based on ANSYS and carried out a topology

optimization analysis of the reel. In this study, based on the above research, the reel model of double-rope winding hoists will be constructed by 3D software. And the deformation of the reel axially will be analyzed by FEA-Simulations, and the maximum deformation of the reel will be reduced and the synchronization and smoothness of double-rope winding hoists will be improved through the improvement of the internal structure of the reel.

2. Modeling of the double-cable winding hoister

Fig. 1 shows a typical 3D model of a double-rope winding hoist reel, and the main material of the reel is Q345A. It is mainly composed of brake disc, reel, rope exit hole, manhole, rope stopper, support column, ribs, two rope wrapping areas and two support wheels. Where d_1 is the diameter of the rope exit hole, d_2 is the diameter of the reel, d_3 is the diameter of the support column. While δ is the thickness of the reel wall, a and c respectively represent the length and width of the thicker ribs. And l_1 is the shortest distance between the two support wheels at the initial moment, while d represents the diameter of the wire rope. The parameters are shown in Table 1.

Table 1. Double rope winding hoist-2JKD-8×4.2 Sample machine parameters

Parameter Name	Value/Unit	Parameter Name	Value/Unit
Diameter of rope outlet hole d_1	200/mm	Diameter of support column d_3	500/mm
Thickness of cylinder shell δ	120/mm	Reinforcement width c	240/mm
Reel diameter d_2	8/m	Pivot wheel distance l_1	3400/mm
Reinforcement length a	350/mm	Wire rope diameter d	180/mm

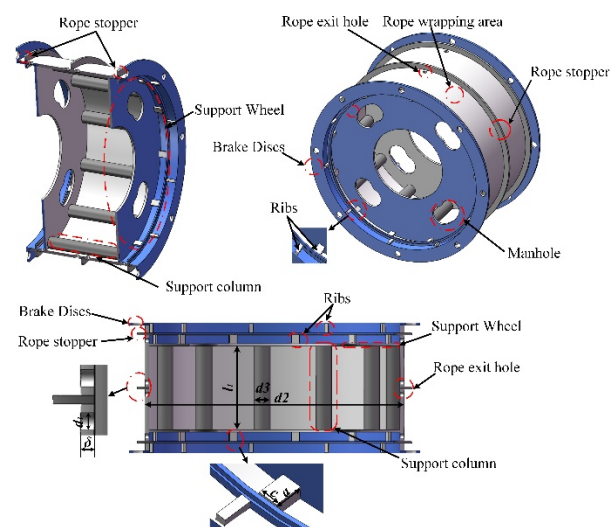


Fig. 1. Internal structure of double-rope hoist

3. Derivation of the double rope winder formula

The double-rope multi-layer hoists use the structure of a thick-shell bullet support, the structure of which is shown in Fig. 2. The thick-shell bullet support has two rope wrapping areas on the left and right, two rope exit holes in each rope-wrapping area and one support wheel.

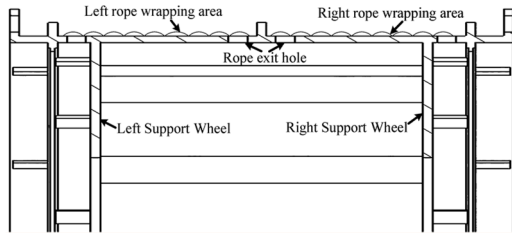


Fig. 2. Thick shell bullet support structure

The double-rope winding hoists are connected to the same cage for hoisting. When the wire rope is at rest before the hoisting starts, the total tension Q_0 of the two wire ropes is shown in Eq.(1),

$$Q_0 = (S + S_0 + pH)g \quad (1)$$

where S represents the rated load. S_0 represents lifting vessel mass. p represents unit mass of steel wire rope. H represents wire rope overhang height. g represents gravitational acceleration.

The total tension on the rope is F_n , where n is the number of wraps, when $n=1$, the rope is under total tension as shown in Eq.(2),

$$F_n = Q_0 = (S + S_0 + pH)g \quad (2)$$

After the wire rope winding a circle, its total tension[2] is affected by the lifting height, lifting speed, lifting acceleration, lifting process of longitudinal vibration[6]-[7] and other factors. At this time the total tension of the lifting system is shown in the Eq.(3),

$$F_n = Q_0 - 4(n-1)\pi R p g + \frac{1}{2}(K-1)Sg + \left[\frac{Q_0}{g} - 4(n-1)\pi R p + 2l_s p + M_1 \right] a_{n-1} \quad (3)$$

where F_n represents total tension of the lifting system. R represents reel radius. K represents tank road lifting resistance coefficient. l_s represents length of dangling wire rope. M_1 represents shifting mass of the sky wheels. a_{n-1} represents lifting acceleration after $n-1$ turns of winding.

Steel wire rope winding process also needs to consider the single-layer and multi-layer winding tension reduction amount on the impact of the radial force of the reel. As single-layer winding, to start the research by rope ring one winding position, the reel radial variable is x_{11} , while winding the n^{th} circle. The i^{th} circle corresponding to the wire rope tension reduction amount is ΔF_{im} . It is shown in Fig.3 and Eq.(4),

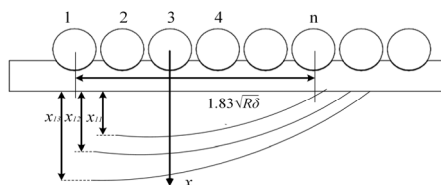


Fig. 3. Single layer winding model

$$\Delta F_{im} = \frac{x_{im}}{R - x_{i(i+1)} - x_{i(i+2)} - \dots - x_{i(n-2)} - x_{i(n-1)}} E_s A_s \quad (i \neq 1) \quad (4)$$

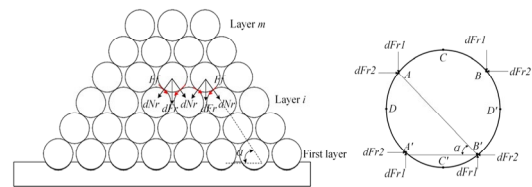
where ΔF_{im} represents reduction in tension on lap i at lap n . x_{im} represents radial deformation at the position of the n^{th} winding turn i . E_s represents longitudinal modulus of elasticity of steel wire rope.

In multi-layer winding[13]-[14] process, the outer layer of wire rope makes the radial force of the reel increase while radial force reduces the radius of the reel, so the inner layer of wire rope appears circumferential relaxation. And the inner layer of wire rope tension is reduced, so the inner layer of radial pressure on the reel is also reduced. Set a total of m winding layer. It corresponds to the i layer of the actual tension size for F'_{im} . The tension size is shown in Eq.(5),

$$F'_{im} = F_i - F_{i(i+1)} - F_{i(i+2)} - \dots - F_{i(m-1)} - F_{i-m} \quad (5)$$

where F_i represents initial tension of the i^{th} layer of wire rope. F_{im} represents tension reduction of layer i caused by winding of m^{th} layer. F'_{im} represents the actual tension of the i^{th} layer.

Multiple layers of wire rope stacked with forces as shown in Fig. 4.



(a) Multi-layer winding force schematic

(b) Separate analysis of multi-layer winding

Fig. 4. Multiple layers of wire rope stacked under stress

The i^{th} layer of wire rope is subjected to the m^{th} layer of the force decomposed into the radial and axial components of the reel as shown in Eqs.(6) and (7),

$$dF_{r1} = \frac{dF_r}{2} = \frac{(F_m - F_{(i+1)m} - F_{(i+2)m} - \dots - F_{(m-1)m})d\theta}{2} \quad (6)$$

$$dF_{r2} = dN_r (\cos \alpha - \mu_r \sin \alpha) = \frac{dF_r (\cos \alpha - \mu_r \sin \alpha)}{2(\sin \alpha + \mu_r \cos \alpha)} \quad (7)$$

where dF_r represents force at m^{th} level on the i^{th} layer. dF_{r1} represents radial component force of layer i on the reel. dF_{r2} represents axial component force of layer i on the reel. μ_r represents friction coefficient between steel wire ropes. N_r represents the support force between the wire rope to generate friction.

The reduction of the chord AA' after the force is applied to the chord length AA' is shown in Eq.(8),

$$\Delta_{im} = \frac{2 \sin \alpha dF_{r1}}{E_r dl_i} = \frac{2 \sin \alpha (F_m - F_{(i+1)m} - F_{(i+2)m} - \dots - F_{(m-1)m})}{E_r [2R + (1 + 2(i-1) \sin \alpha) d]} \quad (8)$$

where E_r represents transverse modulus of elasticity of steel wire rope. α represents wire rope stacking angle. d represents the wire rope diameter. dl_i represents the arc length of the wire rope corresponding to the i^{th} layer winding $d\theta$.

Similarly, the chord length AA' is subjected to a force of dF_{r2} , corresponding to the extension of the chord AA' under the action of F_{r2} as shown in Eq.(9),

$$\Delta'_{i-m} = \sin \alpha v_r \frac{2dF_{i-2}}{E_r d_i} = \frac{2v_r \sin \alpha (F_m - F_{(i+1)m} - F_{(i+2)m} - \dots - F_{(m-1)m}) \cot(\alpha + \gamma)}{E_r [2R + (1 + 2(i-1) \sin \alpha) d]} \quad (9)$$

where v_r represents poisson's ratio of steel wire rope, and $\gamma = \arctan(\mu_r)$.

The amount of radial change produced by the i^{th} layer of wire rope is shown in Eq.(10),

$$\Delta_{i-m} = \Delta'_{i-m} - \Delta''_{i-m} \quad (10)$$

Set the m^{th} layer winding caused by the radial deformation of the reel ΔR_m , the i^{th} layer wire rope corresponding to the total winding radius reduction is shown in Eq.(11),

$$R_{m-m} = \Delta R_m + \Delta_{1m} + \Delta_{2m} + \dots + \frac{1}{2} \Delta_{im} \quad (11)$$

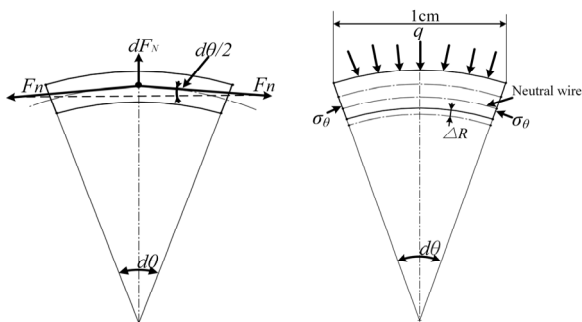
where ΔR_m represents radial deformation of the reel caused by the m^{th} layer winding. R_{m-m} represents reduction of the total winding radius corresponding to the i^{th} layer of wire rope.

From Hooke's law, it is known that the m^{th} layer of wire rope winding causes the reduction of the i^{th} layer of wire rope tension as shown in Eq.(12),

$$F_{i-m} = \frac{Z_{i-m}}{2R + (1 + 2(i-1) \sin \alpha) d} = \frac{2\pi R_{m-m}}{2R + (1 + 2(i-1) \sin \alpha) d} \quad (12)$$

where Z_{i-m} represents the i^{th} layer corresponding to the circumferential length reduction, and $Z_{i-m} = 2\pi R_{m-m}$.

The study of the reel can be based on the model of the thin-walled circular shell[10]-[11], as the spacing between the wire rope is much smaller than the diameter of the reel, the winding process of the wire rope can be regarded as a closed ring of uniform texture [22] acting on the reel. As the wire rope of tension F_n winds to the reel, the reel acts on the combined force of the wire rope as shown in Fig. 5(a). As the unit beam of the reel can be regarded as an elastic base beam [17], so the force analysis of the reel can be based on this. Take a study of the unit beam. The unit beam along the radial direction produced ΔR deformation. In Fig. 5(b) in the reel boundary from the solid line to the dashed line, circumferentially it generated circumferential compressive stress σ_θ , and reel force deformation is shown in Fig. 5(b).



(a) wire rope force (b) Reel unit beam forces

Fig. 5. Force analysis of reel and wire rope

The support force on the wire rope is shown in Eq.(13),

$$dF_N = 2F_n \sin\left(\frac{d\theta}{2}\right) = 2F_n \frac{d\theta}{2} = F_n d\theta \quad (13)$$

where dF_N represents the wire rope is supported by the force of the reel.

The set of loads to which the reel is subjected is shown in Eq.(14),

$$q = \frac{dF'_N}{Rd\theta t_0} = \frac{F_n d\theta}{Rd\theta t_0} = \frac{F_n}{Rt_0} \quad (14)$$

where dF'_N represents pressure in the reel, $dF'_N = dF_N \cdot q$ represents load set. t_0 represents pitch of wire rope, $t_0 = d + e$, d represents diameter of steel wire rope, e represents gap between adjacent rope loops.

Because ΔR and the diameter of the reel compared to the radial displacement of the reel is very small, it can be considered that the distance to the center of the circle at any place on the cross-section is equal to the radius of the reel R . Circumferential strain ϵ_θ is shown in Eq.(15),

$$\epsilon_\theta = \frac{2\pi(R - \Delta R) - 2\pi R}{2\pi R} = -\frac{\Delta R}{R} \quad (15)$$

The balance of circumferential compressive stress and load set is shown in Eqs.(16) and (17),

$$2\sigma_\theta \delta \sin\left(\frac{d\theta}{2}\right) = -qRd\theta \quad (16)$$

$$\sigma_\theta = E_d \epsilon_\theta = -E_d \frac{\Delta R}{R} \quad (17)$$

where δ represents thickness of the reel. E_d represents roll modulus of elasticity.

Where $Rd\theta = 1$, the support force on the reel is F_N as shown in Eq.(18),

$$F_N = 2\delta \sigma_\theta \sin\left(\frac{d\theta}{2}\right) = -\frac{E_d \delta \Delta R}{R^2} = k_1 \Delta R \quad (18)$$

where F_N represents support force on the rollers. k_1 represents foundation reaction coefficient.

The support forces on the reel, the shear forces, and the load set are shown in Fig. 6.

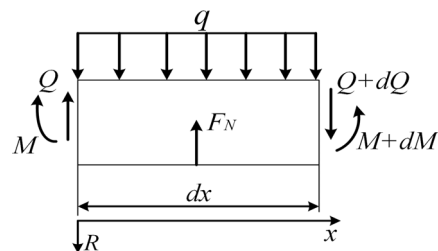


Fig. 6. Sketch of unit beam force analysis

The bending moment, shear force and circumferential force are shown in Eqs.(19) and (20),

$$\begin{cases} \sum Q = -Q + (q - k_1 \Delta R) dx + Q + dQ = 0 \\ \sum M = (q - k_1 \Delta R) dx \frac{dx}{2} + (Q + dQ) dx + M - (M + dM) = 0 \end{cases} \quad (19)$$

$$\begin{cases} M(X) = -D \cdot \frac{d^2 \Delta R}{dx^2} \\ Q(X) = -D \cdot \frac{d^3 \Delta R}{dx^3} \\ C_\theta = -\frac{E_d \delta \Delta R}{R} \end{cases} \quad (20)$$

where D represents flexural stiffness. $M(x)$ represents reel bending moment at any point along x . $Q(x)$ represents reel

shear at any point along x . C_θ represents circumferential force.

4. Finite element analysis of reel deformation and forces

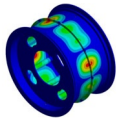
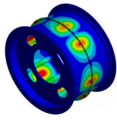
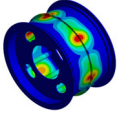
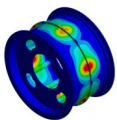
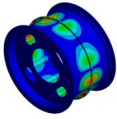
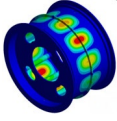
In this section, based on the above derivation, the finite element model of the reel will be constructed, and modal and static analyses will be carried out respectively to obtain the force and deformation of the reel, where the overall parameter values of the reel are shown in Table 2.

Table 2. Summary table of total parameters

Parameter Name	Value/Unit	Parameter Name	Value/Unit
Maximum static tension Q_0	1480/KN	Poisson's ratio of steel wire rope ν_r	0.2
Lifting vessel mass S_0	80/t	Diameter of steel wire rope d	76/mm
Unit mass of steel wire rope p	21.4/kg/m	Pitch of wire rope t_0	78/mm
Wire rope overhang height H	1500/m	Roll modulus of elasticity E_d	2.1×10^5 /Mpa
Gravitational acceleration g	9.8m/s^2	Friction coefficient of steel wire ropes μ_r	0.17
Lifting acceleration a_0	0.75m/s^2	Width of rope winding area B	2.1/m
Length of dangling wire rope l_s	85/m	Cross-sectional area of steel wire rope A_s	2.21×10^3 /mm ²
Number of winding layers n	3	Wire rope stacking angle α	59°
Number of winding layers m	3	Reel radius R	4/m

Boundary constraints are applied to the two end faces of the support wheel and brake disc as fixed supports, and the two rope-wrapping areas of the reel are taken as cylindrical supports. Maximum static tension applied to the rope wrapping area. Under the above conditions, modal analysis is carried out as shown in Table 3.

Table 3. 1st to 6th order modal shapes

Order	Natural frequency (Hz)	Modal shape	Modal Feature
1	234.82		Large and unevenly distributed deformation in the middle
2	235.02		Large middle deformation and more uniform distribution of deformation
3	235.14		Intermediate deformation with a tendency to spread
4	235.36		Uneven distribution of intermediate deformation, with inconsistent peaks along the circumference
5	237.84		Intermediate deformation distribution with reduced deformation
6	238.05		Uneven distribution of total deformation along the circumference

In the lifting process the external load is constantly changing, but at the end of the brake disc and support wheel, the deformations are very small, so the end surfaces of the two parts will be used as boundary conditions. It can be imposed full restraint to the four end surfaces. In order to facilitate the study of the deformation and stress under the force of the reel, the maximum static tension of 1480kN of the wire rope at rest can be taken for the winding area of the reel. Maximum static tension will act on the winding areas as a circumferential force. The corresponding reel displacement cloud diagram and the corresponding equivalent force cloud diagram for the reel is shown in Fig. 7.

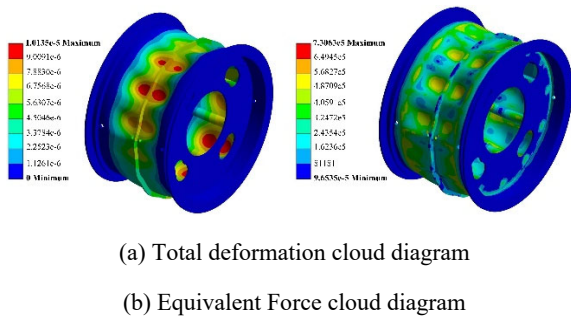


Fig. 7. Initial total deformation and equivalent force clouds

From Fig.7,we can get the conclusion that when the reel is in the work, the total deformation and equivalent force of the reel in the middle part are relatively large. Then the total deformation and equivalent force gradually decrease from the middle position to the two sides. With the maximum static tension of the wire rope, the maximum deformation of the reel is $1.0135 \times 10^{-5} \text{m}$ and the maximum equivalent force is $7.3063 \times 10^5 \text{Pa}$.When reel deformation is too large, it will lead to *Deformation detuning of the wire rope*, which will lead to the tension difference increase of the steel wire rope. This will eventually affect the synchronization of the hoist. As the area of greatest equivalent forces and deformations, the middle area plays the most significant impact on the wire rope in lifting process. So this study will focus on the analysis of the internal structure of the reel change for the impact on the middle of the reel. By changing the internal structure of the reel to reduce the amount of deformation and equivalent force in the middle of the reel.

In order to solve the above problems, this study optimizes the internal structure of the reel by increasing the diameter of the internal support column of the reel and obtains the total deformation and equivalent force clouds of the reel under the same force conditions as shown in Fig. 8

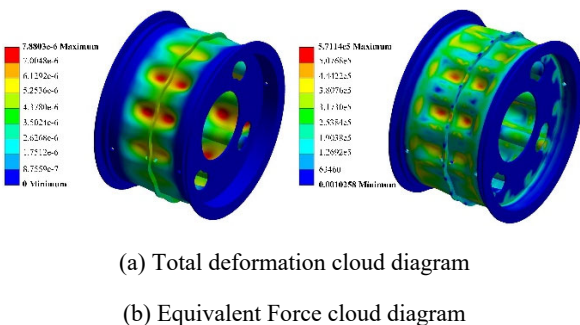


Fig. 8. Cloud diagram after changing internal structure

After improving the internal structure of the reel , it is found that the maximum deformation in the middle of the reel is $7.8803 \times 10^{-6} \text{m}$, which is about 22% lower than the original maximum deformation,and the maximum equivalent force becomes $5.7114 \times 10^5 \text{Pa}$, which is about 21% lower than the original equivalent force value. Through numerical analysis, optimizing the diameter of

the support column inside the reel can well reduce the reel equivalent force and deformation, then reduce the deformation of the reel and lower the tension difference of the wire rope and improve the synchronization and smoothness of the system in the working process.

5. Conclusion

For the application requirements of increasing mining depth, this study chooses the reel model of double-rope winding hoists .Under the maximum static tension of the wire rope, the study takes the reel static force and modal analysis by finite element analysis. It provides the largest equivalent force and deformation parts. And the internal structure of the reel is optimized and improved. The main conclusions are as follows .

1)This study focuses on the analysis of the impact of the reel structure on the wire rope tension difference. By using modal analysis, it gets the conclusion that the 1st to 6th order of the reel frequency is mainly concentrated in 236Hz or so. The maximum total deformation of the reel is mainly concentrated in the middle position, and with a small change in vibration frequency, the deformation of the middle part of the reel will occur in the circumferential movement. The deformation distribution is uneven and the deformation is large or small from time to time .

2) Through the static analysis of the reel, this study concludes that the maximum equivalent force and maximum deformation of the reel occurs in the middle position. After optimizing the diameter of the internal support column of the reel, the maximum total deformation of the reel is reduced from $1.0135 \times 10^{-5} \text{m}$ to $7.8803 \times 10^{-6} \text{m}$, and the maximum equivalent force of the reel is reduced from $7.3063 \times 10^5 \text{Pa}$ to $5.7114 \times 10^5 \text{Pa}$. The two improved parameters are 22% and 21% which are much lower than the original ones. The improvement of the internal structure of the reel has greatly reduced the deformation during the work, thus improving the synchronization and accuracy of the double rope hoisting and reducing the tension difference between the two ropes, providing a reference solution for the future development of double-rope winding hoists depth mining.

This study optimizes the internal structure of a double-rope winding hoists reel based on finite element analysis. The feasibility of the method is verified by using theoretical data and only provides an ideal state of improvement for the further developments of the hoist. The research method and mathematical model do not involve experimental verification, so in the future corresponding experiments can be designed for a more in-depth study.

References

1. Chang X, Peng Y, Zhu Z, et al. Tribological properties of winding hoisting rope between two layers with different sliding parameters. *Adv Mech Eng* 2016; 8: 1687814016679911.
2. Wang J, Pi Y, Hu Y, et al. Modeling and dynamic behavior analysis of a coupled multi-cable double drum winding hoister with flexible guides.

- Mechanism and Machine Theory 2017; 108: 191–208.
3. Wu S, Gong X, He P. Dynamic analysis of multi point winding hoisting system under nonsynchronous movements of wire ropes in deep well. *J Vibroeng* 2021; 23: 512–527.
 4. Antoniak J. Theoretical and run investigation of load distribution onto hoisting ropes in multi rope hoists. *Sci.Issues Tech. Univ. Min.*33 1968 (in Polish).
 5. Li X, Zhu Z, Shen G, et al. Wire Tension Coordination Control of Electro-Hydraulic Servo Driven Double-Rope Winding Hoisting Systems Using a Hybrid Controller Combining the Flatness-Based Control and a Disturbance Observer. *Symmetry-Basel* 2021; 13: 716.
 6. Kaczmarczyk S, Ostachowicz W. Transient vibration phenomena in deep mine hoisting cables. Part 1: Mathematical model. *Journal of Sound and Vibration* 2003;262(2): 219–244.
 7. Kaczmarczyk S, Ostachowicz W. Transient vibration phenomena in deep mine hoisting cables. Part 2: Numerical simulation of the dynamic response. *Journal of Sound and Vibration* 2003;262(2) 245–289.
 8. Peng Y, Chang X, Sun S, et al. The friction and wear properties of steel wire rope sliding against itself under impact load. *Wear* 2018; 400: 194–206.
 9. Yao J, Deng X, Ma C, et al. Investigation of Dynamic Load in Superdeep Mine Hoisting Systems Induced by Drum Winding. *Shock Vib* 2021; 2021: 4756813.
 10. Singh JM, Chattopadhyay A, Rao C. approach towards analysing stresses in a fixed fixed ended long cylindrical winding drum. *Mining Technology* 1984;64:104-110.
 11. Singh JM, Chattopadhyay A, Rao C. Stress analysis in a short cylindrical winding drum. *Mining Technology* 1984;66:400-403.
 12. Otto S, Mupende I, Dietz P. Influence of the hoisting drum winding system on the end plate loads. In: Marjanovic D (ed) *DESIGN 2002: Proceedings of the 7th International Design Conference, Vols 1 and 2*. Zagreb: Univ Zagreb, Faculty Mechanical Engineering & Naval Architecture, pp. 1091–1096.
 13. Dietz P. Design criteria for multilayer wound winch drums following lightweight design principles. In: Marjanovic D (ed) *Design 2004: Proceedings of the 8th International Design Conference, Vols 1-3*. Zagreb: Univ Zagreb, Faculty Mechanical Engineering & Naval Architecture, pp. 15–20.
 14. Dietz P, Lohrengel A, Schwarzer T, et al. Problems related to the design of multi-layer drums for synthetic and hybrid ropes. In: *Innovative ropes and rope applications: A celebration of 175 years of wire rope; Proceedings of the OIPEEC conference 2009 / 3rd International Stuttgart Ropedays*.
 15. Mangalekar S, Bankar V, Chaphale P. Design and Analysis of Central Drum in Mine Hoist. *International Research Journal of Engineering and Technology* 2016;03(06):1111-1114.
 16. Stanisław WOLNY and Sławomir BADURA, «Stress analysis in structural components of the Koepe pulley in hoisting installations», *Engineering Transactions* 2012.
 17. Minjie J, Hanbing W, Hongzhang C, et al. The optimum design of main shaft device of double reels for wrapped hoist. *International Journal of Information and Systems Sciences* 2005;1(3/4):398-405.
 18. Torres B, Paya-Zaforteza I, Calderon PA, et al. Analysis of the strain transfer in a new FBG sensor for Structural Health Monitoring. *Eng Struct* 2011; 33: 539–548.
 19. Chen S. The Optimum Design of A2JK hoist drum based on ANSYS. In: Wang JH, Qi JG (eds) *Materials and Manufacturing, Pts 1 and 2*. Stafa-Zurich: Trans Tech Publications Ltd, pp. 1028–1031.
 20. Hu J, Li J-C, He X, et al. Large Mine Hoist Drum Topology Optimization Design. In: *2016 International Conference on Energy Development and Environmental Protection (edep 2016)*. Lancaster: Destech Publications, Inc, pp. 520–526.
 21. Yu ZL, Li WM. CAE Optimization Design of Mine Hoist Spindle Device. *AMR* 2011; 299–300: 878–882.
 22. Torrance B M. The design of winding drums. *The South African Mechanical Engineer* 1965,15:123-141.